CHEMISTRY
A EUROPEAN JOURNAL

DOI: 10.1002/chem.200902939

Construction of Sn^{IV} Porphyrin/Trinuclear Ruthenium Cluster Dyads Linked by Pyridine Carboxylates: Photoinduced Electron Transfer in the Marcus Inverted Region

Takahiko Kojima,*[a, b] Kakeru Hanabusa,[a] Kei Ohkubo,[a] Motoo Shiro,[c] and Shunichi Fukuzumi*[a, d]

Abstract: Novel conglomerates consisting of saddle-distorted Sn^{IV}(DPP) (H_2DPP = dodecaphenylporphyrin) complexes and μ_3-O-centered and carboxylato-bridged trinuclear Ru^{III} clusters linked by pyridine carboxylates were synthesized and characterized. Sn^{IV}–DPP complexes with Cl^-, OH^-, and 3- and 4-pyridine carboxylates ligands were characterized by spectroscopic methods and X-ray crystallography. Reactions of [Sn(DPP)-(pyridinecarboxylato)$_2$] with trinuclear Ru^{III} clusters gave novel conglomerates in moderate yields. The conglomerates are stable in solution as demonstrated by ^{1}H NMR and electrospray ionization mass spectrometry (ESI-MS) measurements, which show consistent spectra with those expected from their structures, and also by electrochemical measurements, which exhibit reversible multistep redox processes. This stability stems from the saddle distortion of the DPP^{2-} ligand to enhance the Lewis acidity of the Sn^{IV} center that strengthens the axial coordination of the linker. The fast intramolecular photoinduced electron transfer from the Sn^{IV}(DPP) unit to trinuclear Ru^{III} clusters, affording the electron-transfer (ET) state {$Sn(DPP^{\bullet+})$–$Ru^{II}Ru^{III}_2$}, was observed by femtosecond laser flash photolysis. The lifetimes of ET states of the conglomerates were determined to be in the range 98–446 ps, depending on the clusters and energies of the ET states. The reorganization energy of the electron transfer was determined to be 0.58 ± 0.08 eV in light of the Marcus theory of electron transfer. The rate constants of both the photoinduced electron transfer and the back electron transfer in the conglomerates fall in the Marcus inverted region due to the small reorganization energy of electron transfer.

Keywords: cluster compounds · electron transfer · photochemistry · porphyrinoids · ruthenium · tin

Introduction

Photoinduced electron transfer for charge separation is one of the most fundamental events in photosynthesis in order to convert photon energy into chemical energy.[1] A number of donor–acceptor (D–A) linked dyads have been designed and synthesized, and photoinduced electron transfer in the dyads has been examined to mimic the charge separation in the photosynthetic reaction center.[2] Among them, porphyrin-based D–A systems have merited special attention because they perform well in photoinduced electron transfer, giving rise to charge-separated states or electron-transfer (ET) states with relatively long lifetimes.[3–8] The difficulty of time and energy consuming preparations of covalently linked charge separation systems limits the accessibility of further development of photofunctional and related materials. Recently, in order to improve accessibility, supramolecular assemblies having light harvesting functionalities were developed by virtue of noncovalent interactions to self-organize electron donors and electron acceptors.[9–19] However,

[a] Prof. Dr. T. Kojima, K. Hanabusa, Dr. K. Ohkubo, Prof. Dr. S. Fukuzumi
Department of Material and Life Science
Graduate School of Engineering
Osaka University and SORST (JST)
2-1 Yamada-oka, Suita, Osaka 565-0871 (Japan)
Fax: (+81) 6-6879-7370
E-mail: fukuzumi@chem.eng.osaka-u.ac.jp

[b] Prof. Dr. T. Kojima
Department of Chemistry
Graduate School of Pure and Applied Sciences
University of Tsukuba, 1-1-1 Tennoudai, Tsukuba
Ibaraki 305-8571 (Japan)
Fax: (+81) 29-853-4323
E-mail: kojima@chem.tsukuba.ac.jp

[c] Dr. M. Shiro
X-ray Research Laboratory, Rigaku Corporation
3-9-12 Matsubara, Akishima, Tokyo 196-8666 (Japan)

[d] Prof. Dr. S. Fukuzumi
Department of Bioinspired Science
Ewha Womans University, Seoul 120-750 (Korea)

Supporting information for this article is available on the WWW under http://dx.doi.org/10.1002/chem.200902939.

it would be difficult to predict the structures of those assemblies, even based on rational blueprints, and noncovalently linked dyads would be too brittle to maintain their structures in solution.

To improve the accessibility, stability, and reliability of multicomponent donor–acceptor systems, the stronger axial coordination in saddle-distorted porphyrin complexes merits special attention for stabilization the dyads. In this study, we have chosen the saddle-distorted dodecaphenylporphyrin (H_2DPP) as the ligand and Sn^{IV} ion as the metal center, which is a hard Lewis acid, to bind a hard base such as carboxylate oxygen to form stable coordination bonds for the construction of an electron donor, the Sn(DPP) unit. By using this component, stronger coordination of an axial ligand is expected to form stable dyads. As the electron acceptor, μ_3-oxo-centered and carboxylato-bridged trinuclear ruthenium clusters, $[Ru_3(\mu_3\text{-}O)\{OC(O)R\}_6L_3]^{n+}$ (R = general substituent), were used due to their small structural change in the course of redox reactions for smaller reorganization energies.[20–22] These ruthenium clusters have previously been investigated in terms of their multistep and reversible redox behavior and their application to photoconversion of a surface-bound self-assembled monolayers on gold electrodes.[23] m*eso*-Pyridine-coordinated trinuclear ruthenium clusters have been prepared[24] and *intermolecular* photoinduced electron transfer from Zn–porphyrin complexes to triruthenium clusters have been examined.[25] However, examples have not been reported, which demonstrate *intramolecular* photoinduced electron transfer of donor–acceptor dyads consisting of porphyrin compounds and metal clusters to give a charge-separated state.

Herein we report the synthesis and characterization of novel Sn(DPP)/triruthenium cluster conglomerates and the photodynamics of their intramolecular photoinduced electron transfer. The conglomerates undergo efficient photoinduced transfer from the Sn(DPP) unit to the triruthenium cluster with very small reorganization energies to produce the electron-transfer states, which can be clearly detected by laser flash photolysis measurements. This study provides a rational design for obtaining noncovalently linked conglomerates of metalloporphyrins with metal clusters, which exhibit excellent photoinduced electron-transfer performance.

Results and Discussion

Synthesis of Sn^{IV}(DPP) complexes: [Sn(DPP)$(Cl)_2$] (**1**) was synthesized by metallation of dodecaphenylporphyrin (H_2DPP) by using $SnCl_2$ under Ar. Under aerobic conditions, the synthesis of **1** was unsuccessful. [Sn(DPP)$(OH)_2$] (**2**) was obtained by an axial ligand exchange reaction in CH_2Cl_2/THF.[26] Reactions of **2** with 3- and 4-pyridine carboxylic acids (3-PyCOOH and 4-PyCOOH, respectively) in CH_2Cl_2/DMF proceeded smoothly to give [Sn(DPP)(4-PyCO*O*)$_2$] (**3**) and [Sn(DPP)(3-PyCO*O*)$_2$] (**4**).

The chloro complex **1** was characterized by the ^{1}H NMR spectroscopy in $CDCl_3$. The signal assigned to the *o*-phenyl protons of *meso*-phenyl groups was observed at δ = 7.44 ppm as a doublet. Other proton signals were observed around δ = 6.5–6.8 ppm as severely overlapped multiplets. In the case of the hydroxo complex **2**, the signals for *o*-phenyl protons of the *meso*-phenyl groups were observed at δ = 7.33 ppm as a doublet. In addition, a broad signal ascribed to the hydroxo proton was detected at δ = −6.32 ppm, disappearing upon addition of D_2O. The 4-pyridine carboxylato complex **3** exhibited a doublet due to the *o*-protons of the *meso*-phenyl groups at δ = 7.44 ppm and two signals of the pyridine protons of the axial ligands as doublets at δ = 7.87 and 5.56 ppm.

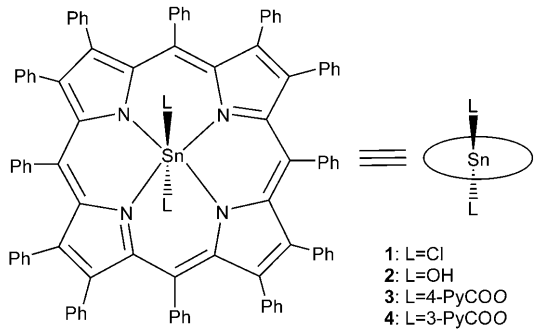

Crystal structures of Sn^{IV}(DPP) complexes: X-ray crystallographic studies of complexes **1**–**4** has made it possible to visualize their molecular structures. ORTEP drawings of those complexes are depicted in Figure 1. Selected bond lengths are listed in Table 1.

The displacements of 24 atoms of the porphyrin core from the porphyrin mean plane in **1**–**4** are given in Figure S1 (see Supporting Information). The displacements indicate that the Sn^{IV}(DPP) complexes depicted in Figure 1 exhibit saddle-distorted structures to a similar extent. The Sn−Cl bond lengths in **1** were 2.391(3) Å for Sn1−Cl1 and 2.254(4) Å for Sn1−Cl2. In the crystal of **2**, two unequivalent molecules are involved in the asymmetric unit and show slightly different bond lengths as listed in Table 1. The Sn−O(H) bond lengths in **2** were found to be 2.038(5) Å for Sn1−O1 and 2.010(5) Å Sn1−O2. The OH ligand (O2) in **2** forms an intermolecular hydrogen bond with a C−H bond of a CH_2Cl_2 molecule of crystallization with an interatomic distance of 3.057 Å for C(H)···O(H). The Sn−O(carboxylato) bond lengths in **3** and **4** were 2.077(2) Å for Sn1−O1 and 2.087(2) Å for Sn1−O2 in **3**, 2.077(2) Å for Sn1−O1 and 2.089(2) Å for Sn1−O2 in **4**. Moreover, planar Sn^{IV}–porphyrin complexes such as [Sn(TPP)$(Cl)_2$] (TPP = tetraphenylporphyrin) and [Sn(TPyP)(4-PyCO*O*)$_2$] (*trans*-diisonicotinate[*meso*-tetrakis(4-pyridyl)porphyrinato]tin(IV)), show longer bond lengths between the Sn^{IV} ions and the axial ligands (Sn−Cl: 2.421(1) Å for [Sn(TPP)$(Cl)_2$],[27] Sn−O: 2.087(3) and 2.091(4) Å for [Sn(TPyP)(4-PyCO*O*)$_2$][28] than the distorted porphyrins. Those observations demonstrate that the distortion of porphyrin plane strengthens the axial coordination, saddle distortion, enhances the Lewis acidity

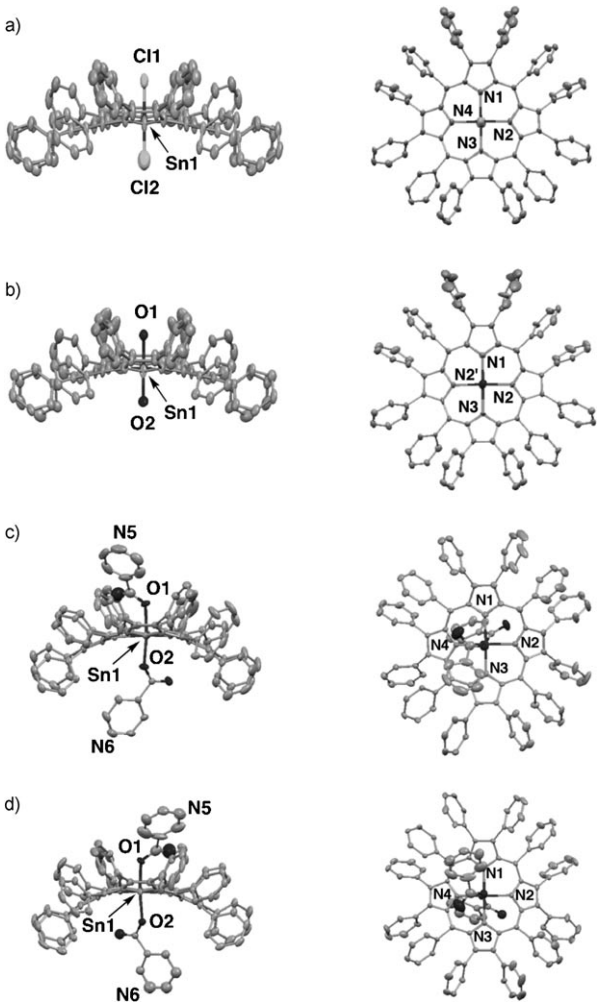

Figure 1. Side views (left) and top views (right) of the crystal structures of Sn^{IV}(DPP) complexes: a) **1**, b) **2**, c) **3**, and d) **4**. Thermal ellipsoids are drawn at the 50% probability level.

Table 1. Selected bond lengths [Å] of **1**–**4**.

	1	2	3	4
Sn1–Cl1	2.391(3)			
Sn1–Cl2	2.254(4)			
Sn1–O1		2.038(5)	2.077(2)	2.077(2)
Sn1–O2		2.010(5)	2.087(2)	2.089(2)
Sn1–N1	2.097(6)	2.122(6)	2.108(4)	2.092(4)
Sn1–N2	2.118(4)	2.121(4)	2.074(5)	2.111(4)
Sn1–N3	2.115(6)	2.115(6)	2.100(4)	2.095(4)
Sn1–N4	2.118(4)	2.121(4)[a]	2.090(4)	2.074(4)

[a] Symmetry operators: x, $y+\frac{1}{2}$, z for N2.

of a metal center due to poor overlap between the $d_{x^2-y^2}$ orbital of the metal center and the lone pairs of pyrrole nitrogen atoms.[29]

Synthesis of conglomerates consist of Sn^{IV}(DPP) complexes and ruthenium clusters: The trinuclear ruthenium clusters, $[Ru_3(\mu_3\text{-}O)(OAc)_6(Py)_2(MeOH)][PF_6]$ (**5**), $[Ru_3(\mu_3\text{-}O)(OBz)_6(H_2O)_3][PF_6]$ (**6**), and $[Ru_3(\mu_3\text{-}O)(OBz)_6(Py)_2(CO)]$ (**7**) (OAc = acetate, Py = pyrindine, Me = methyl, Bz = benzoato) were prepared as reported by Meyer and coworkers.[20] A new cluster $[Ru_3(\mu_3\text{-}O)(OBz)_6(Py)_2(MeOH)][PF_6]$ (**8**) was prepared by the reaction of $[Ru_3(\mu_3\text{-}O)(OBz)_6(Py)_2(CO)]$ with methanol (MeOH) in CH_2Cl_2.[21]

The conglomerates **9**–**12**, made up of the Sn(DPP) complexes and trinuclear Ru^{III} clusters, were prepared by the reaction of acetate-bridged or benzoate-bridged clusters with

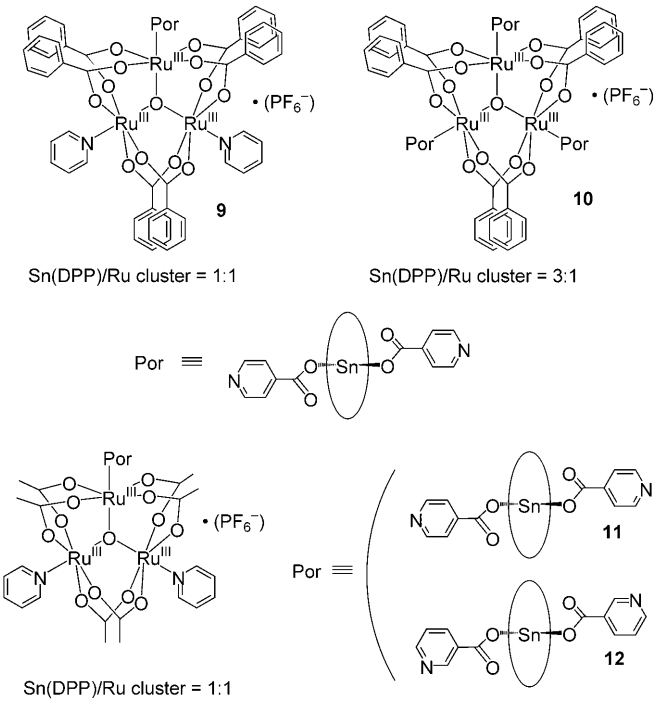

an excess amount of **3** or **4** in a mixture of CH_2Cl_2 and acetone. After the reaction, the crude products were purified by column chromatography on a biobeads (S-X1) eluted with CH_2Cl_2. Formation of conglomerates was confirmed by electrospray ionization mass spectrometry (ESI-MS) to observe molecular ion peak clusters with isotopic patterns.

For conglomerates with paramagnetic trinuclear Ru^{III} clusters, the NMR spectra became ambiguous due to the influence of unpaired electrons in the clusters. Therefore, ^{1}H NMR spectra were measured after one-electron reduction by adding hydrazine as a reductant to form a mixed-valent $Ru^{II}Ru^{III}_2$ state, which was diamagnetic due to strong antiferromagnetic coupling between the two Ru^{III} centers in the $S=\frac{1}{2}$ spin state through the μ_3-oxo group.[30] Peaks were assigned by ^{1}H-^{1}H COSY, as presented in the Experimental Section. In the case of one-electron-reduced **9**, two sets of signals derived from the 4-$PyCOO^-$ ligands were observed at $\delta=8.66$ (2-H) and 6.20 ppm (3-H), and also at $\delta=7.86$ (2-H) and 5.57 ppm (3-H) as doublets. The former set of signals are assigned to those of the 4-$PyCOO^-$ ligand binding to the ruthenium trinuclear cluster as the bridging ligand. The latter set of signals is almost intact with respect to the signals in **3** and are thus ascribed to those of the terminal 4-

$PyCOO^-$ ligand. Peak integration of two sets of phenyl groups of benzoato at $\delta = 7.61$ (*o*-H), 7.08 ppm (*m*- and *p*-H) and $\delta = 7.31$ (*o*-H), 6.98 (*p*-H), 6.78 ppm (*m*-H)[31] allowed us to determine the ratio of those signals to be 1:2 in the one-electron-reduced conglomerate **9**, indicating its twofold symmetry. However, in the one electron reduced conglomerate **10**, the signals due to the phenyl groups of the benzoato ligands were observed at $\delta = 6.87$ (*o*-H), 6.73 (*o*-H),[31] 6.35 ppm (*p*-H) for one mono-substituted phenyl group, supporting its threefold symmetry. These results lend credence to the formation of discrete 1:1 and 3:1 conglomerates **9** and **10**, respectively, indicating that those conglomerates are stable in solution.

Electrochemical measurements: Redox potentials of **3** and **4** were determined by differential pulse voltammetry (DPV), because of their low solubility in benzonitrile (PhCN). Redox potentials of conglomerates **9**–**12** were obtained by cyclic voltammetry (CV) and DPV measurements, and those for **9** and **10** as representative examples are shown in Figure 2. Based on the redox potentials of the conglomerates, the energy levels of charge-separated states were determined as the difference between the first oxidation, and the first reduction potentials are summarized in Table 2. The conglomerates exhibited three reversible redox waves within the range from −1.20 to +1.25 V. The Ru cluster moieties showed one reversible reduction wave due to $Ru^{III}{}_3$/$Ru^{II}Ru^{III}{}_2$ redox couple (0.03 V for **9**, 0.11 V for **10**, −0.13 V for **11**, and −0.11 V for **12**) and one reversible oxidation wave ascribed to the $Ru^{III}{}_3$/$Ru^{III}{}_2Ru^{IV}$ redox couple (1.06 V for **9**, 1.06 V for **10**, 0.90 V for **11**, and 0.93 V for **12**). The Sn(DPP) moieties exhibited reversible reduction waves (−0.91 V for **9**, −0.90 V for **10**, −0.89 V for **11**, and −0.91 V for **12**) due to the Sn(DPP)/Sn($DPP^{\bullet-}$) redox couple and the oxidation waves ascribed to the Sn(DPP)/Sn($DPP^{\bullet+}$) redox couple (1.06 V for **9**, 1.06 V for **10**, 1.04 V for **11**, and 1.04 V for **12**), which are overlapped with the oxidation waves of Ru cluster moieties in the cases of **9** and **10**. The current intensity ratios of reduction waves derived from the Sn–porphyrin moieties and the Ru cluster moieties were 3:1 for **10** and 1:1 for **9**, **11**, and **12**. These ratios are consistent with those of the numbers of Sn–porphyrin moieties and Ru cluster moieties in the conglomerates. Together with the results from NMR spectroscopy as described above, this result indicates that the conglomerates are stable in solution and during the course of redox reactions.

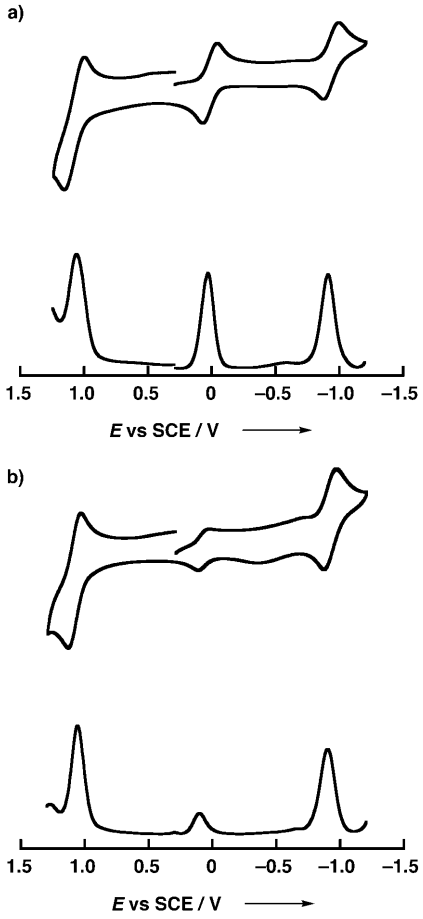

Figure 2. Cyclic voltammograms (upper traces) and differential pulse voltammograms (lower traces) of conglomerates a) **9** and b) **10** in PhCN (0.1 M $TBAPF_6$ as an electrolyte).

Table 2. Redox potentials of Sn^{IV}(DPP)/Sn^{IV}($DPP^{\bullet-}$) (E_{ox}) and $Ru^{III}{}_3$/$Ru^{II}Ru^{III}{}_2$ (E_{red}) in **9**–**12** in PhCN (versus SCE) with the energy levels of the ET states of the conglomerates.

	E_{ox} [V]	E_{red} [V]	Energy level of ET state [eV][a]
9	1.06	0.03	1.03
10	1.06	0.11	0.95
11	1.04	−0.13	1.17
12	1.04	−0.11	1.15

[a] Determined as ($E_{ox} - E_{red}$).

UV/Vis spectra of the conglomerates in PhCN are shown as black lines in Figure S2 (see Supporting Information). The conglomerates show the Soret and the Q bands derived from the Sn–porphyrin moieties. Their absorption bands are slightly shifted compared to those of Sn(DPP) precursor complexes, indicating the formation of conglomerates in solution. When the conglomerates are reduced by hydrazine, the Ru cluster moiety shows a broad intervalence charge transfer (IVCT) band at 900 nm, which is evidence for the formation of a mixed valence state (red lines in Figure S2 in Supporting Information).[20,24] The absorbance intensity ratio of the Q-band of the Sn(DPP) moiety and the IVCT band of the Ru cluster was consistent with that of the number of Sn(DPP) moieties and Ru clusters in each conglomerate.

However, the electron-transfer oxidation of the conglomerates with $[Ru(bpy)_3][PF_6]_3$ (bpy = 2,2′-bipyridine) used as an oxidant result in the appearance of broad absorptions around 850 nm, which were assigned to those of the cation radicals of Sn(DPP) moieties in the conglomerates as shown in Figure 3. The oxidation of **3** by $[Ru(bpy)_3]^{3+}$ under the same conditions resulted in the emergence of broad absorp-

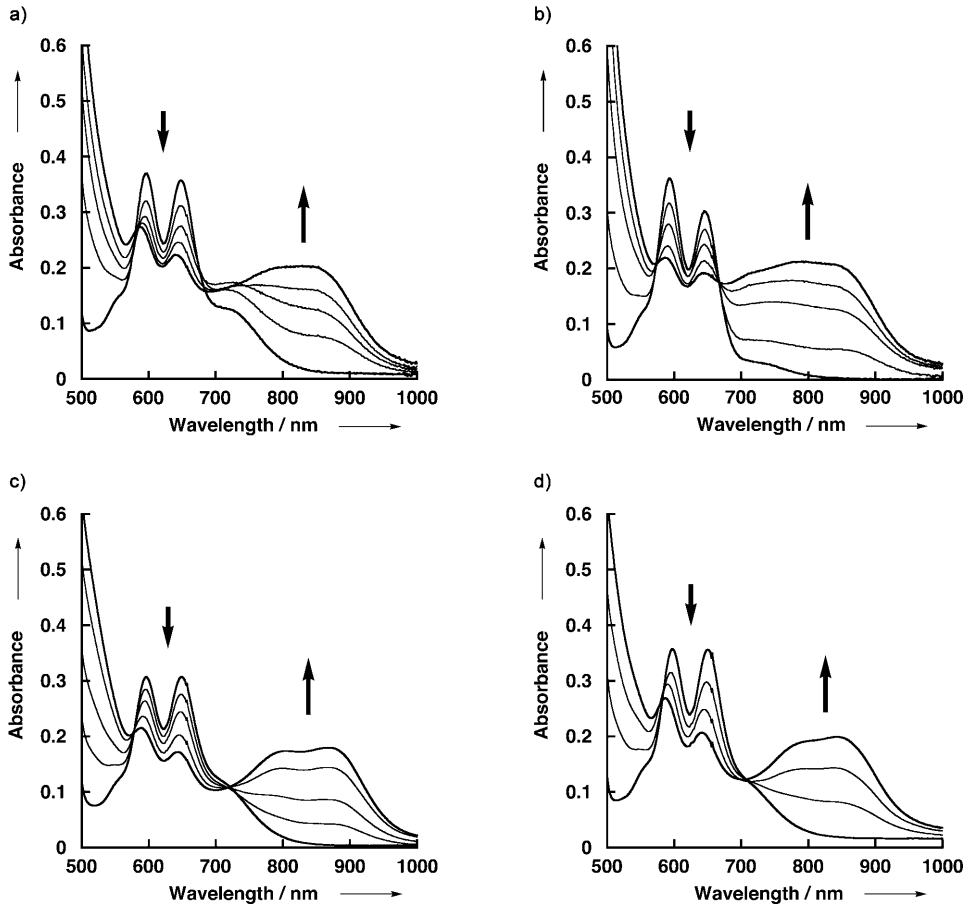

Figure 3. UV spectra of conglomerates a) **9**, b) **10**, c) **11**, and d) **12** after oxidation with $[Ru(bpy)_3][PF_6]_3$ in PhCN at room temperature.

tions exhibiting the absorption maxima at 779 and 850 nm with decreasing the absorptions at 594 and 649 nm as shown in Figure S3a (see Supporting Information). The oxidation of **4** under the same conditions allowed us to observe similar spectral changes as shown in Figure S3b (see Supporting Information), exhibiting the absorption maximum at 853 nm. The spectral change observed in the oxidations of **3** and **4** to generate $[Sn(DPP^{\bullet-})(4\text{-}PyCOO)_2]^+$ and $[Sn(DPP^{\bullet-})(3\text{-}PyCOO)_2]^+$, respectively, in PhCN lends credence to the formation of the same species in the conglomerates.

Photoexcited states of conglomerates: The energies of the singlet excited states of **9–12** were determined to be 1.88 eV based on the absorption and fluorescence maxima in PhCN. Both $[Sn(DPP)(4\text{-}PyCO\mathit{O})_2]$ and $[Sn(DPP)(3\text{-}PyCO\mathit{O})_2]$ exhibited the same absorption and fluorescence maxima under the same conditions. The energies of triplet excited states of **9–12** were estimated to be 1.29 eV from the phosphorescence maximum of $[Sn(DPP)(4\text{-}PyCO\mathit{O})_2]$ at 960 nm (See Figure S4 in Supporting Information).

Femtosecond transient absorption spectra of $[Sn(DPP(4\text{-}PyCO\mathit{O})_2)$ in PhCN are shown in Figure S5a (see Supporting Information). The absorption band assigned to the singlet excited state of $[Sn(DPP)(4\text{-}PyCO\mathit{O})_2]$ appeared at 850 nm. The rate constant of intersystem crossing was determined from the time profile of its decay at 850 nm and is $1.2\times10^8\ s^{-1}$ ($\tau=8.3$ ns) as shown in Figure S5(b) (see Supporting Information).

Photodynamics of conglomerates: Femtosecond transient absorption spectra of conglomerate **10** in PhCN upon photoexcitation at 430 nm is shown in Figure 4 with time profiles of the decay of absorption at 850 nm. Those of **9**, **11**, and **12** are also given in Figures S6, S7, and S8 (see Supporting Information), respectively. The absorption band in the range of 783–830 nm is cut because the detector changed at around 800 nm from the visible region to the near-infrared (NIR) region. In conglomerate **10** (3:1), the absorption at 850 nm due to the singlet excited state of the $[Sn(DPP)(4\text{-}PyCO\mathit{O})_2]$ moiety decayed much faster than that of authentic $[Sn(DPP)(4\text{-}PyCO\mathit{O})_2]$ as shown in Figure S9 (see Supporting Information). This indicates the occurrence of photoinduced electron transfer from the Sn(DPP) moiety to the trinuclear Ru cluster in **10**. At 100 ps, the transient absorption spectrum exhibited a new band at around 900 nm, which is ascribed to the ET state ($Sn(DPP^{\bullet+})$–$Ru^{II}Ru^{III}_2$) by comparison with UV/Vis spectra of $Sn(DPP^{\bullet+})$–Ru^{III}_3 and Sn(DPP)–$Ru^{II}Ru^{III}_2$, produced by the ET oxidation of Sn(DPP)–Ru^{III}_3 with $[Ru(bpy)_3]^{3+}$ and reduction with hydrazine, respectively. The convolution of absorption spectra of $Sn(DPP^{\bullet+})$ and the mixed valent $Ru^{II}Ru^{III}_2$ cluster agrees well with that observed at 100 ps after laser illumination, as depicted in Figure 5. This supports the formation of the ET state ($Sn(DPP^{\bullet+})$–$Ru^{II}Ru^{III}_2$) in the conglomerate.

From the analysis of the time profile of the absorbance at 850 nm in Figure 4, the rate constants of forward electron transfer (k_{ET}) and back electron transfer (k_{BET}) were determined to be $k_{ET}=8.6\times10^{10}\ s^{-1}$ and $k_{BET}=3.3\times10^9\ s^{-1}$, respectively. The other slow component is recognized in the absorption time profile. This is assigned to the intersystem crossing of uncoordinated $[Sn(DPP)(4\text{-}PyCO\mathit{O})_2]$, which would be derived from dissociation from the conglomerate in the course of photoexcitation.

Femtosecond laser flash photolysis was also performed for the other conglomerates **10–12** under the same condi-

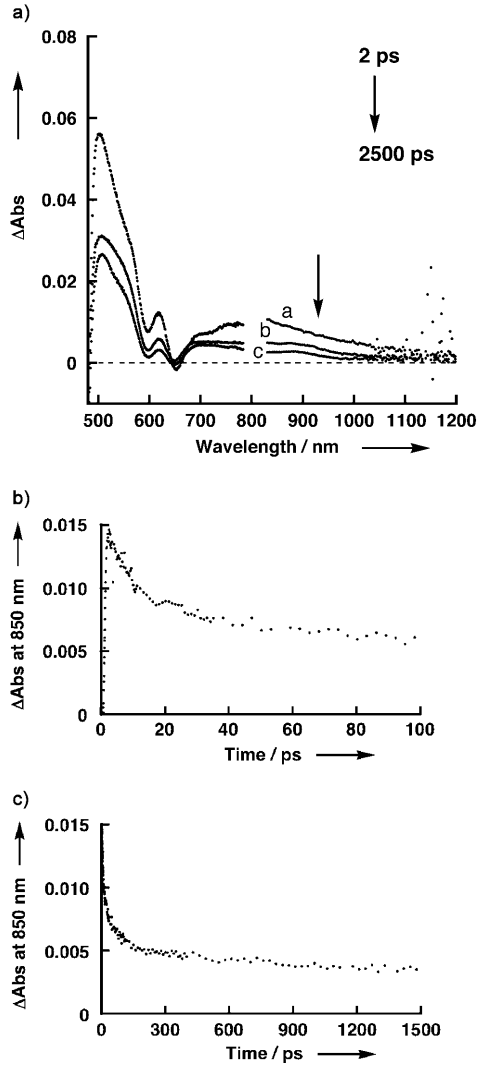

Figure 4. a) Transient absorption spectra of the conglomerate **10** in PhCN measured at 2 (trace a), 100 (trace b), 2500 ps (trace c) after laser excitation at 430 nm. b) and c) Time profiles at 850 nm.

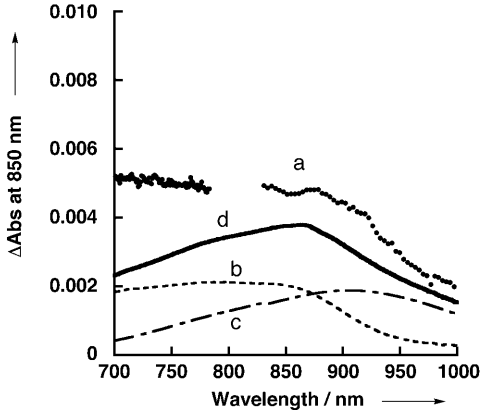

Figure 5. Transient absorption spectrum of conglomerate **10** in PhCN measured at 100 ps (trace a). Absorption spectra of $Sn(DPP^{\bullet+})$–Ru^{III}_3 (trace b), Sn(DPP)–$Ru^{II}Ru^{III}_2$ (trace c), and superposition of $Sn(DPP^{\bullet+})$–Ru^{III}_3 and Sn(DPP)–$Ru^{II}Ru^{III}_2$ (trace d).

tions. In all cases, the formation of the ET states was recognized as supported by the convolution of the corresponding spectra, as mentioned in the case of **9**. The ET and back electron transfer (BET) rate constants in the conglomerates are summarized in Table 3.

Table 3. Driving forces and rate constants of ET and BET of conglomerates.

	$-\Delta G_{ET}$ [eV]	$-\Delta G_{BET}$ [eV]	k_{ET} [s^{-1}]	k_{BET} [s^{-1}]
9	0.85	1.03	8.6×10^{10}	3.3×10^{9}
10	0.93	0.95	9.1×10^{10}	6.5×10^{9}
11	0.71	1.17	7.7×10^{10}	2.2×10^{9}
12	0.73	1.15	7.1×10^{10}	1.0×10^{9}

On the basis of the results described above, the energy diagrams of photodynamics in the Sn(DPP)–Ru^{III}_3 conglomerates in PhCN are shown in Figure 6. In each case, the Sn-

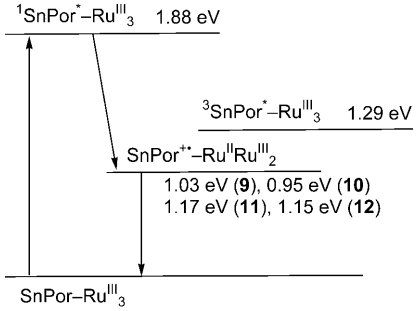

Figure 6. Energy diagram of conglomerates **9**–**12**.

(DPP) moiety is excited to form the singlet excited state at the energy level of 1.88 eV. This singlet excited state undergoes fast intramolecular photoinduced electron transfer to the corresponding trinuclear Ru^{III} cluster in the conglomerate to afford an ET state ($Sn(DPP^{\bullet+})$–$Ru^{II}Ru^{III}_2$) within 11–14 ps. The ET state decays through back electron transfer to recover the ground state, Sn(DPP)–Ru^{III}_3. The lifetimes of the ET states are determined on the basis of the rate constants of back electron transfer to be 305, 154, 446, and 98 ps for **9**–**12**, respectively.

Analysis of electron transfer based on the Marcus theory: The reorganization energy (λ) of electron transfer can be determined from the driving-force dependence of $\log(k_{ETorBET})$ for photoinduced electron transfer and back electron transfer, respectively, in light of the Marcus theory of electron transfer as expressed in Equation (1).[32,33]

$$k_{ET/BET} = \left(\frac{4\pi^3}{h^2\lambda k_B T}\right) V^2 \exp\left(-\frac{(\Delta G_{ET/BET} + \lambda)^2}{4\lambda k_B T}\right) \quad (1)$$

The fitting of the results to Equation (1) afforded the reorganization energy of 0.58 eV and $V = 28.2\ cm^{-1}$ as shown as the solid line in Figure 7. Both ET and BET occur in the

Marcus inverted region. This reorganization energy of electron transfer is relatively small in comparison with other related dyads giving rise to charge-separated states or electron-transfer states.[34]

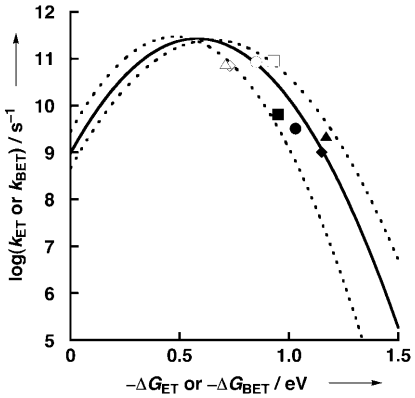

Figure 7. Driving force dependence of log k_{ET} (open marks) or k_{BET} (closed marks) for intramolecular electron transfer of conglomerates in PhCN at 298 K; **9** (circle), **10** (square), **11** (triangle) and **12** (rhombus). The fit of the curve based on the Marcus theory of electron transfer [Eq. (1)] is shown by the solid line with $\lambda = 0.58$ eV and $V = 28.2$ cm^{-1} and the dotted lines with $\lambda = 0.50$ and 0.66 eV and $V = 28.2$ cm^{-1}.

Importance of the saddle distortion: A planar Sn^{IV}–porphyrin [Sn(TPP)(4-PyCO*O*)$_2$] was synthesized to examine the effects of the saddle distortion on the photoinduced electron-transfer reactions. In sharp contrast to the case of **3**, the complex decomposed upon laser illumination to most likely give [Sn(TPP)(OH)$_2$] in PhCN. Moreover, conglomerates including [Sn(TPP)(4-PyCO*O*)$_2$] were synthesized by reactions with **5** or **8** to form [{Sn(TPP)(4-PyCO*O*)}{μ-(4-PyCOO)}{Ru_3(μ$_3$-O)(OAc)$_6$(Py)$_2$}]$^+$ (**13**) and [{Sn(TPP)(4-PyCO*O*)}{μ-(4-PyCOO)}{Ru_3(μ$_3$-O)(OBz)$_6$(Py)$_2$}]$^+$ (**14**), in similar manner to that of **9** and **11**. Their formation was confirmed by ESI-MS in acetone to detect peak clusters assigned to their molecular ions at 1808.6 for **13** (calcd. 1808.05) and at 2180.6 for **14** (calcd. 2180.17). In the course of laser flash photolysis, the UV/Vis absorption spectra of these conglomerates in PhCN changed to exhibit that of [Sn(TPP)(OH)$_2$] even in the case of [Sn(TPP)(4-PyCO*O*)$_2$]. These results indicate that coordination bonds between the axial ligands and the Sn^{IV}(TPP) moiety are cleaved under photoirradiation to give rise to the decomposition of the conglomerates. This is due to the weaker axial coordination in planar porphyrin complexes compared to those in the distorted counterparts.[29] Thus, it is clearly demonstrated that the saddle distortion of the porphyrin ligand is indispensable for the construction of stable conglomerates involving a stronger axial coordination to link a donor and an acceptor.

Conclusion

We have described the synthesis and characterization of novel conglomerates consisting of the saddle-distorted Sn^{IV}-(DPP) unit and μ$_3$-O-centered and carboxylato-bridged trinuclear Ru^{III} clusters linked by pyridine carboxylates. The conglomerates are stable in solution as demonstrated by ^{1}H NMR and ESI-MS measurements to show consistent spectra with those expected from their structures and also by electrochemical measurements to exhibit reversible multistep redox processes. This stability stems from the saddle distortion of the DPP^{2-} ligand to enhance the Lewis acidity of the Sn^{IV} center, which strengthens the axial coordination of the linker. Femtosecond laser flash photolysis allowed us to observe the occurrence of fast intramolecular photoinduced electron transfer from the Sn(DPP) unit to trinuclear Ru^{III} cluster, affording the electron-transfer state Sn-($DPP^{\bullet+}$)–$Ru^{II}Ru^{III}_2$. The ET state of the conglomerates showed lifetimes ranging from 98 to 446 ps, depending on the clusters and linkers employed. Analysis based on the Marcus theory of electron transfer allowed us to determine the reorganization energy in the electron transfer to be 0.58 ± 0.08 eV, which is comparable to Zn^{II}–porphyrin-based dyads.[35] The analysis also demonstrated that the rate constants of both the photoinduced electron transfer and the back electron transfer in the conglomerates fall in the Marcus inverted region, in which the larger driving force of electron transfer, the slower the rates become.[36] This research may pave a way to the development of novel photofunctional molecules and materials based on coordinatively linked donor–acceptor light-harvesting components.

Experimental Section

Materials: Chemicals were purchased from commercial sources and used without further purification, unless otherwise noted. CH_2Cl_2 was distilled over CaH_2 before use. Toluene was distilled over sodium benzophenone ketyl and used for the synthesis of H_2DPP. PhCN used for spectral measurements was distilled over P_2O_5 before use. H_2DPP was synthesized as reported previously.[37]

Synthesis of Sn porphyrin complexes: The Sn^{IV}(DPP) complexes were synthesized on the basis of procedures reported by Sanders and co-workers[38] for **1** and **2** and by Crossley and co-workers for **3** and **4**.[39]

[Sn(DPP)(Cl)$_2$] (1): H_2DPP (350 mg, 0.29 mmol) was heated to reflux with anhydrous tin(II) chloride (115 mg, 0.61 mmol) in pyridine (35 mL) under nitrogen for 6 h and then heated to reflux under air for 24 h. After removal of pyridine under reduced pressure, the residue was dissolved in CH_2Cl_2, and the solution was filtrated to remove the precipitate. The filtrate was washed with water in a separatory funnel, and the organic layer was dried over anhydrous sodium sulfate. The solvent was removed with by rotary evaporation. The residue was purified by column chromatography on activated alumina using CH_2Cl_2/MeOH (8:1 v/v) as the eluent. The third green fraction was collected, and the solution was evaporated to dryness to obtain a green solid (at this stage, Sn(DPP)(OH)$_2$). Recrystallization of the solid from $CHCl_3$/CH_3CN gave green crystals of **1**. Yield 220 mg (54%); elemental analysis calcd (%) for $C_{92}H_{60}N_4Cl_2Sn{\cdot}CH_2Cl_2{\cdot}CHCl_3$: C 69.89, H 3.93, N 3.47; found: C 70.15, H 4.07, N 3.68; ^{1}H NMR ($CDCl_3$): $\delta = 7.44$ (d, $J = 7.5$ Hz, 8H; *meso*-phenyl *o*-H), 6.85–6.44 ppm (m, 52H; *meso*-phenyl *m*-, *p*-H, β-phenyl H); MALDI-TOF-MS (matrix: dithranol): *m*/*z* calcd for $C_{92}H_{60}N_4ClSn$:

1375.3; found: 1375.1 $[M-Cl]^+$; UV/Vis (CH_2Cl_2): λ_{max} (ε) = 459 (2.17×10^5), 588 (1.29×10^4), 646 nm ($9.88\times10^3\,M^{-1}cm^{-1}$).

[Sn(DPP)(OH)$_2$] (2): Complex **1** (150 mg, 0.11 mmol) was dissolved in CH_2Cl_2/THF (3:1 v/v) with an aqueous solution of K_2CO_3 (5 mM, 1 mL) and heated to reflux overnight. The solvent was evaporated, and the crude product was dissolved in CH_2Cl_2. After filtration, the filtrate was washed with water in a separatory funnel and then dried over anhydrous sodium sulfate. Recrystallization of the solid from CH_2Cl_2/CH_3CN (1:2 v/v) gave green crystals of **2**. Yield 118 mg (78%); elemental analysis calcd (%) for $C_{92}H_{62}N_4O_2Sn{\cdot}2CH_2Cl_2$: C 73.12, H 4.31, N 3.63; found: C 73.39, H 4.72, N 3.72; ^{1}H NMR ($CDCl_3$): δ = 7.33 (d, J = 8 Hz, 8H; *meso*-phenyl *o*-H), 6.80–6.45 (m, 52H; *meso*-phenyl *m*-, *p*-H, β-phenyl H), −6.32 ppm (s, 2H). MALDI-TOF-MS (matrix: dithranol): *m*/*z* calcd for $C_{92}H_{60}N_4OHSn$:1357.2; found: 1357.3 $[M-(OH)]^+$;); UV/Vis (CH_2Cl_2): λ_{max} (ε) = 455 (2.38×10^5), 584 (1.56×10^4), 648 nm ($8.80\times10^3\,M^{-1}cm^{-1}$).

[Sn(DPP)(4-PyCO*O*)$_2$] (3): A solution of **2** (150 mg, 0.11 mmol) in CH_2Cl_2 (100 mL) was added to a solution of 4-pyridinecarboxylic acid (200 mg, 1.62 mmol) in DMF (20 mL). The mixture was stirred overnight at room temperature and then evaporated to dryness under reduced pressure. Recrystallization of the residue from CH_2Cl_2/CH_3CN gave green crystals of **3**. Yield 122 mg (70%); elemental analysis calcd (%) for $C_{104}H_{68}N_6O_4Sn{\cdot}H_2O$: C 77.95, H 4.40, N 5.24; found: C 78.23, H 4.54, N 5.43; ^{1}H NMR ($CDCl_3$): δ = 7.87 (d, J = 6 Hz, 4H; axial pyridyl *o*-H), 7.44 (d, J = 8 Hz, 8H; *meso*-phenyl *o*-H), 6.84–6.56 (m, 52H; *meso*-phenyl *m*-, *p*-H, β-phenyl H). 5.56 ppm (d, J = 6 Hz, 4H; axial pyridyl *m*-H); MALDI-TOF-MS (matrix; dithranol): *m*/*z* calcd for $C_{98}H_{64}N_5O_2Sn$ 1462.3; found: 1462.3 $[M-(PyCO*O*)]^+$; UV/Vis (PhCN): λ_{max} (ε) = 466 (1.82×10^5), 597 (1.41×10^4), 653 nm ($1.40\times10^4\,M^{-1}cm^{-1}$.

[Sn(DPP)(3-PyCO*O*)$_2$] (4): Complex **4** was prepared by using the same procedure as for **3**, but using 3-pyridinecarboxylic acid as an axial ligand instead of 4-pyridinecarboxylic acid. Yield: 131 mg (75%) elemental analysis calcd (%) for $C_{104}H_{68}N_6O_4Sn{\cdot}2H_2O$: C 77.09, H 4.48, N 5.19; found: C 77.31, H 4.65, N 5.29; ^{1}H NMR ($CDCl_3$): δ = 8.08 (d, J = 5 Hz, 2H; pyridyl 6-C*H*), 7.43 (d, J = 8 Hz, 8H; *meso*-phenyl *o*-H), 6.86 (s, 2H; pyridyl 2-C*H*), 6.80–6.54 (m, 53H; *meso*-phenyl *m*-, *p*-H, β-phenyl H, pyridyl 5-C*H*). 6.08 ppm (d, J = 8 Hz, 2H; pyridyl 4-C*H*). MALDI-TOF-MS (matrix; dithranol): *m*/*z* calcd for $C_{98}H_{64}N_5O_2Sn$ 1462.3; found: 1462.1 $[M-(PyCO*O*)]^+$; UV/Vis (PhCN): λ_{max} (ε) = 464 (1.72×10^5), 594 (9.57×10^3), 647 nm ($7.97\times10^3\,M^{-1}cm^{-1}$).

Synthesis of trinuclear Ru clusters: $[Ru_3(\mu_3\text{-}O)(OAc)_6(Py)_2(MeOH)][PF_6]$ (**5**), $[Ru_3(\mu_3\text{-}O)(OBz)_6(H_2O)_3][PF_6]$ (**6**), and $[Ru_3(\mu_3\text{-}O)(OBz)_6(Py)_2(CO)]$ (**7**) were synthesized using literature procedures.[20,21]

[Ru$_3$(μ$_3$-O)(OBz)$_6$(Py)$_2$(MeOH)][PF$_6$] (8): Br_2 (1 mL) in CH_2Cl_2 (0.15 M, threefold excess) was added to a solution of **7** (50 mg, 0.041 mmol) in CH_2Cl_2 (50 mL). The solution was stirred for 30 min, and the solvent was removed under reduced pressure. A suspension of the residue in methanol (40 mL) was heated to reflux until a homogeneous blue solution was observed. The solution was allowed to cool slowly and a solution of NH_4PF_6 (40 mg, 0.24 mmol) in a minimum amount of methanol was slowly added. The resulting solution was cooled to 0°C and filtered. A blue solid was collected, washed with a small amount of methanol and diethyl ether, and then air dried. Yield 40 mg (71%); elemental analysis calcd (%) for $C_{53}Ru_3H_{44}O_{16}N_2PF_6{\cdot}H_2O{\cdot}CH_3OH$: C 45.32, H 3.52, N 1.96; found: C 45.02, H 3.30, N, 2.12; ESI-MS (in acetone): *m*/*z* calcd for $C_{52}H_{40}N_2O_{13}Ru_3$ requires 1204.98; found: 1205.30 $[M-(CH_3OH)]^+$.

Synthesis of conglomerate [{Sn(DPP)(4-PyCO*O*)}{μ-(4-PyCOO)}{Ru$_3$-(μ$_3$-O)(OBz)$_6$(Py)$_2$}][PF$_6$] (9): Cluster **8** (8.2 mg, 0.0063 mmol) was slowly added as a solid to a solution of **3** (100 mg, 0.063 mmol) in CH_2Cl_2 (20 mL). The solution was stirred for 24 h with protection from light. The reaction mixture was purified by chromatography on a biobeads (S-X1; Bio-RAD) column using CH_2Cl_2 as the eluent. The first green fraction was collected and the solution was evaporated to dryness to obtain a green solid of **9**. Yield 9.6 mg (52%); elemental analysis calcd (%) for $C_{156}H_{108}N_8O_{17}SnRu_3PF_6{\cdot}2CH_2Cl_2$: C 61.15, H 3.64, N, 3.61; found: C 61.47, H 3.69, N 3.70; ^{1}H NMR ($CDCl_3$): δ = 9.40 (d, J = 5 Hz, 4H; pyridyl *o*-H), 8.66 (d, J = 6 Hz, 2H; μ-pyridyl(axial) *m*-H). 8.01 (t, J = 8 Hz, 2H; pyridyl *p*-H), 7.86 (d, J = 6 Hz, 2H; pyridyl(axial) *m*-H), 7.85 (t, J = 8 Hz, 4H; pyridyl *m*-H), 7.61 (d, J = 6 Hz, 4H; phenyl(benzoate) *o*-H), 7.55 (d, J = 8 Hz, 8H; *meso*-phenyl *o*-H), 7.31 (d, J = 8 Hz, 8H; phenyl-(benzoate) *o*-H), 7.08 (t, J = 8 Hz, 6H; phenyl(benzoate) *m*-, *p*-H), 6.98 (t, J = 7 Hz, 4H; phenyl(benzoate) *p*-H), 6.88–6.50 (m, 60H; *meso*-phenyl *m*-, *p*-H, β-phenyl H, phenyl(benzoate) *p*-H), 6.20 (d, J = 7 Hz, 2H; μ-pyridyl(axial) *o*-H), 5.57 ppm(d, J=6 Hz, 2H; pyridyl(axial) *o*-H); ESI-MS (in acetone): *m*/*z* calcd for $C_{156}H_{108}N_8O_{17}SnRu_3$: 2789.41; found: 2789.43 $[M]^+$; UV/Vis (PhCN): λ_{max} = 466, 597, 648 nm.

Synthesis of conglomerate [{Sn(DPP)(4-PyCOO)}$_3${μ-(4-PyCOO)}$_3${Ru$_3$-(μ$_3$-O)(OBz)$_6$}][PF$_6$] (10): Complex **3** (200 mg, 0.126 mmol) in a CH_2Cl_2/acetone (15 mL; 1:1 v/v) mixture was heated to reflux and cluster **6** (5.23 mg, 0.0042 mmol) in CH_2Cl_2/acetone (15 mL; 1:1 v/v) was slowly added through an addition funnel under protection from light. The mixture was heated to reflux for 12 h. The solution was evaporated and the crude product was purified by chromatography on a biobeads (S-X1) column using CH_2Cl_2 as the eluent. The first green fraction was collected and the solution was evaporated to dryness to obtain a green solid of **10**. Yield 9.8 mg (42%); elemental analysis calcd (%) for $C_{354}H_{234}N_{18}O_{25}Sn_3Ru_3PF_6{\cdot}4CH_2Cl_2$: C 68.43, H 3.88, N 4.01; found: C 68.79, H 4.20, N 3.60; the four CH_2Cl_2 moleucles were confirmed by ^{1}H NMR; ^{1}H NMR ($CDCl_3$): δ = 8.37 (d, J = 7 Hz, 6H; μ-pyridyl(axial) *m*-H), 7.85 (d, J = 7 Hz, 6H; pyridyl(axial) *m*-H), 7.63–7.47 (m, 24H; *meso*-phenyl *o*-H), 6.87 (d, J = 7 Hz, 12H; phenyl(benzoate) *o*-H), 6.84–6.46 (m, 168H; *meso*-phenyl *m*-, *p*-H, β-phenyl H, phenyl(benzoate) *m*-H), 6.35 (t, J = 8 Hz, 6H; phenyl(benzoate) *p*-H), 6.07 (d, J = 6 Hz, 6H; μ-pyridyl(axial) *o*-H), 5.55 ppm (d, J = 6 Hz, 6H; pyridyl(axial) *o*-H); UV/Vis (PhCN): λ_{max} = 464, 595, 648 nm.

Synthesis of conglomerate [{Sn(DPP)(4-PyCO*O*)}{μ-(4-PyCOO)}{Ru$_3$-(μ$_3$-O)(OAc)$_6$(Py)$_2$}][PF$_6$] (11): Conglomerate **11** was prepared using the same procedure as **9**, but with **5** instead of **8**. Yield: 5.49 mg (34%); elemental analysis calcd (%) for $C_{126}H_{96}N_8O_{17}SnRu_3PF_6{\cdot}2CH_2Cl_2$: C 56.30, H 3.69, N 4.10; found: C 56.52, H 3.74, N 4.17; ^{1}H NMR ($CDCl_3$): δ = 9.38 (d, J = 5 Hz, 4H; pyridyl(axial) *o*-H), 8.71 (d, J = 5 Hz, 2H; μ-pyridyl(axial) *m*-H), 7.91 (t, J = 7 Hz, 4H; pyridyl *m*-H), 7.70 (d, J = 5 Hz, 12H; pyridyl(axial) *m*-H), 7.69 (t, J = 7 Hz, 2H; pyridyl *p*-H), 6.89–6.40 (m, 8H; *meso*-phenyl *o*-H), 7.53 (m, 52H; *meso*-phenyl *m*-, *p*-H, β-phenyl H), 5.99 (d, J = 5 Hz, 2H; μ-pyridyl(axial) *o*-H), 5.59 ppm (d, J = 5 Hz, 2H; pyridyl(axial) *o*-H); ESI-MS (in acetone): *m*/*z* calcd for $C_{126}H_{96}N_8O_{17}SnRu_3$ 2416.2; found: 2416.5 $[M]^+$; UV/Vis (PhCN): λ_{max} = 463, 593, 648 nm.

Synthesis of conglomerate [{Sn(DPP)(3-PyCO*O*)}{μ-(3-PyCOO)}{Ru$_3$-(μ$_3$-O)(OAc)$_6$(Py)$_2$}][PF$_6$] (12): Conglomerate**12** was prepared using the same procedure as **9**, but with **5** instead of **8** and **4** instead of **3**. Yield: 6.61 mg (41%); elemental analysis calcd (%) for $C_{126}H_{96}N_8O_{17}SnRu_3PF_6{\cdot}3CH_2Cl_2{\cdot}H_2O$: C 54.67, H 3.70, N 3.95; found: C 54.44, H 3.87, N, 4.06; ^{1}H NMR ($CDCl_3$): δ = 9.36 (d, J = 5 Hz, 4H; pyridyl *o*-H), 9.04 (d, J = 6 Hz, 1H; μ-pyridyl(axial) 6-C*H*), 8.73 (s, 1H; μ-pyridyl(axial) 2-C*H*), 8.06 (d, J = 5 Hz, 1H; pyridyl(axial) 6-C*H*), 7.94 (t, J = 7 Hz, 2H; pyridyl *p*-H), 7.68 (t, J = 7 Hz, 4H; pyridyl *m*-H), 7.58–7.46 (m, 8H; *meso*-phenyl *o*-H), 6.87 (s, 1H; pyridyl(axial) 2-C*H*), 6.83–6.40 (m, 54H; pyridyl(axial) 5-C*H*, *meso*-phenyl *m*-, *p*-H, β-phenyl H, μ-pyridyl(axial) 5-C*H*), 6.05 (d, J = 7 Hz, 1H; μ-pyridyl(axial) 4-C*H*), 5.52 ppm (d, J = 8 Hz, 1H; pyridyl(axial) 4-C*H*); ESI-MS (in acetone): *m*/*z* calcd for $C_{126}H_{96}N_8O_{17}SnRu_3$: 2416.2; found: 2416.8 $[M]^+$; UV/Vis (PhCN): λ_{max} = 466, 597, 650 nm.

X-ray crystallography: Single crystals of **1**–**4** were mounted on glass capillaries by silicon grease and diffraction data were collected on a Rigaku Mercury CCD diffractometer with a rotating anode X-ray tube with graphite-monochromated $Mo_{K\alpha}$ radiation (λ = 0.7107 Å) at −150°C (**1** and **2**) and −160°C (**3** and **4**). The structures were solved by direct methods (SIR 97)[40] and refined by full-matrix least-squares method on F^2 using the CrystalStructure program package.[41] Crystallographic data for **1**–**4** are also summarized in Table 4. CCDC-702272 (**1**·$CHCl_3$),[42] 752023 (**2**·CH_2Cl_2), 752024 (**3**), and 752025 (**4**) contain the supplementary crystallographic data for this paper. These data can be obtained free of charge from The Cambridge Crystallographic Data Centre via www.ccdc.cam.ac.uk/data_request/cif.

Electrochemical measurements: Cyclic voltammetry (CV) and differential pulse voltammetry (DPV) were performed on an ALS 630B electro-

Table 4. Crystallographic data for **1**·$CHCl_3$, **2**·CH_2Cl_2, **3**, and **4**.

	1·$CHCl_3$	**2**·CH_2Cl_2	**3**	**4**
formula	$C_{93}H_{61}N_4Cl_5Sn$	$C_{93}H_{64}N_4O_2Cl_2Sn$	$C_{102}H_{68}N_6O_4Sn$	$C_{102}H_{68}N_6O_4Sn$
fw	1530.5	1459.15	1560.39	1560.39
crystal system	orthorhombic	orthorhombic	triclinic	triclinic
space group	*Pnma*	*Pnma*	$P\bar{1}$	$P\bar{1}$
T [K]	123	123	113	113
a [Å]	11.7235(2)	11.311(1)	15.524(4)	15.581(3)
b [Å]	28.4110(7)	28.456(1)	16.719(5)	16.742(4)
c [Å]	21.1529(5)	21.505(1)	18.112(5)	18.058(4)
α [°]			111.8210(19)	111.3114(12)
β [°]			101.7880(17)	101.7344(16)
γ [°]			109.2962(19)	109.4819(11)
V [Å^3]	7045.5(3)	6921.7(7)	3820.8(19)	3844.3(15)
Z	4	4	2	2
reflns	44110	46477	16728	29962
obsrvd reflns	6450	6410	12822	16667
parameters	476	462	1037	992
$R1$[a] [$I>2.0\sigma(I)$]	0.083	0.068	0.078	0.072
$wR2$[b] (all data)	0.236	0.221	0.194	0.181
GOF	1.036	1.092	1.101	1.096

[a] $R1=\Sigma||F_o|-|F_c||/\Sigma|F_o|$. [b] $wR2=[\Sigma(w(F_o^2-F_c^2)^2)/\Sigma w(F_o^2)^2]^{1/2}$.

chemical analyzer in deaerated MeCN containing 0.1 M $[(n\mathrm{Bu}_4)\mathrm{N}]PF_6$ ($TBAPF_6$) as a supporting electrolyte at 298 K. A conventional three-electrode cell was used with a platinum working electrode (surface area of 0.3 mm^2) and a platinum wire as the counter electrode. The Pt working electrode (BAS) was routinely polished with BAS polishing alumina suspension and rinsed with acetone before use. The potentials were measured with respect to the $Ag/AgNO_3$ (0.01 M) reference electrode. All of the potentials (versus Ag/Ag^+) were converted to values versus SCE by adding 0.29 V.[43] All of the electrochemical measurements were carried out under an atmospheric pressure of argon.

Phosphorescence measurements: Phosphorescence of an Ar saturated solution of [Sn(DPP)(4-PyCO*O*)$_2$] in Et_2O/isopentane/EtOH/EtI (5:5:2:2; 0.5 mL) in a quartz tube (3 mm in diameter) in liquid nitrogen was measured using a SPEX Fluorolog τ3 fluorescence spectrophotometer by excitation at 650 nm. A photomultiplier (Hamamatsu Photonics model R5509–72) was used to detect emission in the near-IR region.

Spectroscopic measurements: Absorption spectra were measured on a SHIMADZU UV-3100 spectrophotometers or a Hewlett Packard 8453 diode array spectrophotometer at room temperature. Fluorescence spectra were measured by using an absolute PL quantum yield measurement system (Hamamatsu photonics, C9920–02) by excitation at 482 nm. ^{1}H NMR spectra were obtained on a JEOL AL-300 spectrometers and chemical shift (ppm) was determined by using the residual solvent peak as a reference. MALDI-TOF-MS and ESI-MS measurements were performed on a Kratos Compact MALDI I (Shimadzu) and a Perkin–Elmer API-150 spectrometers, respectively.

Femtosecond laser flash photolysis: Femtosecond transient absorption spectroscopy experiments on solutions of **3**, **4**, **9**, **10**, **11**, and **12** in PhCN were conducted using an ultrafast source: Integra-C (Quantronix Corp.), an optical parametric amplifier: TOPAS (Light Conversion Ltd.) and a commercially available optical detection system: Helios provided by Ultrafast Systems LLC. The source for the pump and probe pulses were derived from the fundamental output of Integra-C (780 nm, 2 mJ per pulse and fwhm = 130 fs) at a repetition rate of 1 kHz. 75% of the fundamental output of the laser was introduced into TOPAS which has optical frequency mixers resulting in tunable range from 285 nm to 1660 nm, while the rest of the output was used for white-light generation. Prior to generating the probe continuum, a variable neutral density filter was inserted in the path in order to generate a stable continuum, then the laser pulse was fed to a delay line that provides an experimental time window of 3.2 ns with a maximum step resolution of 7 fs. In our experiments, a wavelength at 430 nm of TOPAS output, which is the fourth harmonic of the signal or idler pulses, was chosen as the pump beam. Since this TOPAS output consists of not only the desirable wavelength but also unnecessary wavelengths, the latter were deviated using a wedge prism with wedge angle of 18°. The desirable beam was irradiated at the sample cell with a spot size of 1 mm diameter where it was merged with the white probe pulse in a close angle (< 10°). The probe beam after passing through the 2 mm sample cell was focused on a fiber optic cable that was connected to a CCD spectrograph for recording the time-resolved spectra (410–800, 800–1650 nm). Typically, 2500 excitation pulses were averaged for 5 seconds to obtain the transient spectrum at a set delay time. Kinetic traces at appropriate wavelengths were assembled from the time-resolved spectral data.

Acknowledgements

This work was supported by Grants-in-Aid (Nos. 21750146 and 20108010), a Global COE program, "the Global Education and Research Center for Bio-Environmental Chemistry" from the Japan Society of Promotion of Science (JSPS) and the Ministry of Education, Science, Technology of Japan, the Iketani Science and Technology Foundation, and by KOSEF/MEST through WCU project (R31-2008-000-10010-0).

[1] *The Photosynthetic Reaction Center* (Eds.: J. Deisenhofer, J. R. Norris), Academic Press, San Diego, **1993**.
[2] a) M. R. Wasielewski, *Chem. Rev.* **1992**, *92*, 435; b) M. R. Wasielewski, *J. Org. Chem.* **2006**, *71*, 5051.
[3] a) D. Gust, T. A. Moore in *The Porphryin Handbook, Vol. 8* (Eds.: K. M. Kadish, K. Smith, R. Guilard), Academic Press, San Diego, **2000**, p. 153; b) D. Gust, T. A. Moore, A. L. Moore, *Acc. Chem. Res.* **2001**, *34*, 40; c) P. A. Liddell, G. Kodis, A. L. Moore, T. A. Moore, D. Gust, *J. Am. Chem. Soc.* **2002**, *124*, 7668; d) J. Andréasson, G. Kodis, T. Ljungdahl, A. L. Moore, T. A. Moore, D. Gust, J. Mrtensson, B. Albinsson, *J. Phys. Chem. A* **2003**, *107*, 8825; e) P. A. Liddell, G. Kodis, J. Andrasson, L. de La Garza, S. Bandyopadhyay, R. H. Mitchell, T. A. Moore, A. L. Moore, D. Gust, *J. Am. Chem. Soc.* **2004**, *126*, 4803; f) R. E. Palacios, G. Kodis, S. L. Gould, L. de La Garza, A. Brune, D. Gust, T. A. Moore, A. L. Moore, *ChemPhysChem* **2005**, *6*, 2359; g) G. Kodis, Y. Terazono, P. A. Liddell, J. Andrasson, V. Garg, M. Hambourger, T. A. Moore, A. L. Moore, D. Gust, *J. Am. Chem. Soc.* **2006**, *128*, 1818.
[4] a) H. Imahori, K. Tamaki, D. M. Guldi, C. Luo, M. Fujitsuka, O. Ito, Y. Sakata, S. Fukuzumi, *J. Am. Chem. Soc.* **2001**, *123*, 2607; b) H. Imahori, D. M. Guldi, K. Tamaki, Y. Yoshida, C. Luo, Y. Sakata S. Fukuzumi, *J. Am. Chem. Soc.* **2001**, *123*, 6617; c) D. M. Guldi, H. Imahori, K. Tamaki, Y. Kashiwagi, H. Yamada, Y. Sakata, S. Fukuzumi, *J. Phys. Chem. A* **2004**, *108*, 541; d) S. Fukuzumi, *Org. Biomol. Chem.* **2003**, *1*, 609; e) H. Imahori, *Org. Biomol. Chem.* **2004**, *2*, 1425.
[5] a) S. Fukuzumi, *Bull. Chem. Soc. Jpn.* **2006**, *79*, 177; b) H. Imahori, *Bull. Chem. Soc. Jpn.* **2007**, *80*, 621; c) S. Fukuzumi, *Phys. Chem. Chem. Phys.* **2008**, *10*, 2283.
[6] a) S. Chakraborty, T. J. Wadas, H. Hester, C. Flaschenreim, R. Schmehl, R. Eisenberg, *Inorg. Chem.* **2005**, *44*, 6284; b) S. Chakra-

borty, T. J. Wadas, H. Hester, R. Schmehl, R. Eisenberg, *Inorg. Chem.* **2005**, *44*, 6865.

[7] a) K. Ohkubo, H. Kotani, J. Shao, Z. Ou, K. M. Kadish, G. Li, R. K. Pandey, M. Fujitsuka, O. Ito, H. Imahori, S. Fukuzumi, *Angew. Chem.* **2004**, *116*, 871; *Angew. Chem. Int. Ed.* **2004**, *43*, 853; b) J. R. Stromberg, A. Marton, H. L. Kee, C. Kirmaier, J. R. Diers, C. Muthiah, M. Taniguchi, J. S. Lindsey, D. F. Bocian, G. J. Meyer, D. Holten, *J. Phys. Chem. A* **2007**, *111*, 15464.

[8] a) K. Maruyama, A. Osuka, *Pure Appl. Chem.* **1990**, *62*, 1511; b) D. Gust, T. A. Moore, *Science* **1989**, *244*, 35; c) D. Gust, T. A. Moore, *Top. Curr. Chem.* **1991**, *159*, 103; d) D. Gust, T. A. Moore, A. L. Moore, *Acc. Chem. Res.* **1993**, *26*, 198; e) M. R. Wasielewski, *Chem. Rev.* **1992**, *92*, 435; f) M. N. Paddon-Row, *Acc. Chem. Res.* **1994**, *27*, 18; g) N. Sutin, *Acc. Chem. Res.* **1983**, *16*, 275; h) A. J. Bard, M. A. Fox, *Acc. Chem. Res.* **1995**, *28*, 141; i) T. J. Meyer, *Acc. Chem. Res.* **1989**, *22*, 163; j) P. Piotrowiak, *Chem. Soc. Rev.* **1999**, *28*, 143.

[9] a) J.-M. Lehn, *Supramolecular Chemistry: Concepts and Perspectives*, VCH, Weinheim, **1995**; b) J. L. Sessler, B. Wang, S. L. Springs, C. T. Brown in *Comprehensive Supramolecular Chemistry* (Eds.: J. L. Atwood, J. E. D. Davies), Pergamon, New York, **1996**.

[10] C. J. Chang, J. D. K. Brown, M. C. Y. Chang, E. A. Baker, D. G. Nocera in *Electron Transfer in Chemistry, Vol. 3* (Ed.: V. Balzani), Wiley-VCH, Weinheim, **2001**, pp. 409–461.

[11] a) C. A. Hunter, J. K. M. Sanders, G. S. Beddard, S. Evans, *J. Chem. Soc. Chem. Commun.* **1989**, 1765; b) H. L. Anderson, C. A. Hunter, J. K. M. Sanders, *J. Chem. Soc. Chem. Commun.* **1989**, 226.

[12] a) P. J. F. de Rege, S. A. Williams, M. J. Therien, *Science* **1995**, *269*, 1409; b) A. Harriman, D. J. Magda, J. L. Sessler, *J. Chem. Soc. Chem. Commun.* **1991**, 345; c) J. L. Sessler, B. Wang, A. Harriman, *J. Am. Chem. Soc.* **1995**, *117*, 704; d) A. Berman, E. S. Izraeli, H. Levanon, B. Wang, J. L. Sessler, *J. Am. Chem. Soc.* **1995**, *117*, 8252.

[13] a) F. D′Souza, N. P. Rath, G. R. Deviprasad, M. E. Zandler, *Chem. Commun.* **2001**, 267; b) F. D′Souza, G. R. Deviprasad, M. E. El-Khouly, M. Fujitsuka, O. Ito, *J. Am. Chem. Soc.* **2001**, *123*, 5277; c) F. D′Souza, G. R. Deviprasad, M. S. Rahman, J. Choi, *Inorg. Chem.* **1999**, *38*, 2157; d) F. D′Souza, M. E. Zandler, P. M. Smith, G. R. Deviprasad, K. Arkady, M. Fujitsuka, O. Ito, *J. Phys. Chem. A* **2002**, *106*, 649.

[14] a) T. Da Ros, M. Prato, D. M. Guldi, M. Ruzzi, L. Pasimeni, *Chem. Eur. J.* **2001**, *7*, 816; b) F. D′Souza, *J. Am. Chem. Soc.* **1996**, *118*, 923; c) M. E. El-Khouly, L. M. Rogers, M. E. Zandler, G. Suresh, M. Fujitsuka, O. Ito, F. D′Souza, *ChemPhysChem* **2003**, *4*, 474; d) F. D′Souza, G. R. Deviprasad, M. E. Zandler, M. E. El-Khouly, M. Fujitsuka, O. Ito, *J. Phys. Chem. B* **2002**, *106*, 4952.

[15] H. F. M. Nelissen, M. Kercher, L. De Cola, M. C. Feiters, R. J. M. Nolte, *Chem. Eur. J.* **2002**, *8*, 5407.

[16] a) P. Lainé, F. Bedioui, E. Amouyal, V. Albin, F. Berruyer-Penaud, *Chem. Eur. J.* **2002**, *8*, 3162; b) P. Laine', F. Bedioui, P. Ochsenbein, V. Marvaud, M. Bonin, E. Amouyal, *J. Am. Chem. Soc.* **2002**, *124*, 1364.

[17] Y. Kashiwagi, H. Imahori, Y. Araki, O. Ito, K. Yamada, Y. Sakata, S. Fukuzumi, *J. Phys. Chem. A* **2003**, *107*, 5515.

[18] K. Okamoto, S. Fukuzumi, *J. Phys. Chem. B* **2005**, *109*, 7713.

[19] T. Hasobe, H. Imahori, P. V. Kamat, T. K. Ahn, S. K. Kim, D. Kim, A. Fujimoto, T. Hirakawa, S. Fukuzumi, *J. Am. Chem. Soc.* **2005**, *127*, 1216.

[20] J. A. Baumann, D. J. Salmon, S. T. Wilson, T. J. Meyer, W. E. Hatfield, *Inorg. Chem.* **1978**, *17*, 3342.

[21] M. Abe, Y. Sasaki, T. Yamaguchi, T. Ito, *Bull. Chem. Soc. Jpn.* **1992**, *65*, 1585.

[22] a) T. Ito, T. Hamaguchi, H. Nagino, T. Yamaguchi, H. Kido, I. S. Zavarine, T. Richmond, J. Washington, C. P. Kubiak, *J. Am. Chem. Soc.* **1999**, *121*, 4625; b) M. Abe, T. Michi, A. Sato, T. Kondo, W. Zhou, S. Ye, K. Uosaki, Y. Sasaki, *Angew. Chem.* **2003**, *115*, 3018; *Angew. Chem. Int. Ed.* **2003**, *42*. 2912.

[23] M. Abe, T. Masuda, T. Kondo, K. Uosaki, Y. Sasaki, *Angew. Chem.* **2005**, *117*, 420; *Angew. Chem. Int. Ed.* **2005**, *44*. 416.

[24] K. Ota, H. Sasaki, T. Matsui, T. Hamaguchi, T. Yamaguchi, T. Ito, H. Kido, C. P. Kubiak, *Inorg. Chem.* **1999**, *38*, 4070.

[25] M. Itou, M. Otake, Y. Araki, O. Ito, H. Kido, *Inorg. Chem.* **2005**, *44*, 1580.

[26] In $CHCl_3$, complex **2** was converted to $[Sn(DPP)(Cl)_2]$ by axial exchange reaction owing to trace amount of HCl in $CHCl_3$.

[27] D. M. Collins, W. R. Scheidt, J. L. Hoard, *J. Am. Chem. Soc.* **1972**, *94*, 6689.

[28] H. Kim, H. J. Jo, J. Kim, S. Kim, D. Kim, K. Kim, *CrystEngComm* **2005**, *7*, 417.

[29] T. Kojima, T. Nakanishi, T. Honda, R. Harada, M. Shiro, S. Fukuzumi, *Eur. J. Inorg. Chem.* **2009**, 727.

[30] H. Kobayashi, N. Uryu, I. Mogi, R. Miyamoto, Y. Ohba, M. Iwaizumi, Y. Sasaki, A. Ohto, T. Ito, *Bull. Chem. Soc. Jpn.* **1995**, *68*, 2551.

[31] These peaks overlapped with other signals in 1D ^{1}H NMR spectra and were assigned on the basis of detection of cross peaks in their ^{1}H-^{1}H COSY spectra.

[32] a) R. A. Marcus, *Annu. Rev. Phys. Chem.* **1964**, *15*, 155; b) R. A. Marcus, N. Sutin, *Biochim. Biophys. Acta* **1985**, *811*, 265; c) R. A. Marcus, *Angew. Chem.* **1993**, *105*, 1161; *Angew. Chem. Int. Ed. Engl.* **1993**, *32*, 1111; *Angew. Chem.* **1993**, *105*, 1161.

[33] a) M. Bixon, J. Jortner in *Electron Transfer, Part 1* (Eds.: J. Jortner, M. Bixon), Wiley, New York, **1999**, pp. 35–202; b) J. Ulstrup, J. Jortner, *J. Chem. Phys.* **1975**, *63*, 4358.

[34] a) H. Imahori, K. Tamaki, D. M. Guldi, C. Luo, M. Fujitsuka, O. Ito, Y. Sakata, S. Fukuzumi, *J. Am. Chem. Soc.* **2001**, *123*, 2607; b) L. Martín-Gomis, K. Ohkubo, F. Fernández-Lázaro, S. Fukuzumi, A. Sastre-Santos, *J. Phys. Chem. C* **2008**, *112*, 17694; c) F. D′Souza, R. Chitta, K. Ohkubo, M. Tasior, N. K. Subbaiyan, M. E. Zandler, M. K. Rogacki, D. T. Gryko, S. Fukuzumi, *J. Am. Chem. Soc.* **2008**, *130*, 14263.

[35] a) K. Okamoto, Y. Mori, H. Yamada, H. Imahori, S. Fukuzumi, *Chem. Eur. J.* **2004**, *10*, 474; b) H. Imahori, K. Tamaki, D. M. Guldi, C. Luo, M. Fujitsuka, O. Ito, Y. Sakata, S. Fukuzumi, *J. Am. Chem. Soc.* **2001**, *123*, 2607.

[36] For another rare example of the photoinduced electron-transfer process in the Marcus inverted region, see: J. L. Sessler, E. Karnas, S. K. Kim, Z. Ou, M. Zhang, K. M. Kadish, K. Ohkubo, S. Fukuzumi, *J. Am. Chem. Soc.* **2008**, *130*, 15256.

[37] W. Jentzen, M. C. Simpson, J. D. Hobbs, X. Song, T. Ema, N. Y. Nelson, C. J. Medforth, K. M. Smith, M. Veyrat, M. Mazzanti, R. Ramasseul, J.-C. Marchon, T. Takeuchi, W. A. Goddard III, J. A. Shelnutt, *J. Am. Chem. Soc.* **1995**, *117*, 11085.

[38] J. H. Hawley, N. Bampos, J. K. M. Sanders, *Chem. Eur. J.* **2003**, *9*, 5211.

[39] P. R. Brotherhood, R. A. Wu, P. Turner, M. J. Crossley, *Chem. Commun.* **2007**, 225.

[40] SIR 97, Program Suite for the Solution and Refinement of Crystal Structures from Diffraction Data, G. M. Sheldrick, University of Göttingen, Göttingen, **1997**.

[41] CrystalStructure 3.7.0, Crystal Structure Analysis Package, Rigaku and Rigaku/MSC (2000–2005), The Woodlands, TX 77381.

[42] This data was reported in the Supporting Information of the following paper: T. Kojima, K. Hanabusa, K. Ohkubo, M. Shiro, S. Fukuzumi, *Chem. Commun.* **2008**, 6513.

[43] C. K. Mann, K. K. Barnes, *Electrochemical Reactions in Non-aqueous Systems*, Mercel Dekker, New York, **1970**.

Received: October 23, 2009
Published online: March 5, 2010

